Available online at www.sciencedirect.com
SCIENCE DIRECT®
ELSEVIER
Palaeogeography, Palaeoclimatology, Palaeoecology 209 (2004) 281–301
PALAEO
www.elsevier.com/locate/palaeo

Late Pleistocene–Holocene oceanographic variability in the Okhotsk Sea: geochemical, lithological and paleontological evidence

S.A. Gorbarenko[a,*], J.R. Southon[b], L.D. Keigwin[c], M.V. Cherepanova[d,1], I.G. Gvozdeva[a]

[a] *Russian Academy of Sciences, Pacific Oceanological Institute, Baltiyskaya St. 43, Vladivostok 690041, Russia*
[b] *Lawrence Livermore National Laboratory, Livermore, CA 94551-9900, USA*
[c] *Woods Hole Oceanographic Institution, Woods Hole, MA 02543, USA*
[d] *Institute of Biology and Soil Science, FEBRAS, Prospect Stoletiya Vladivostoka, 159, Vladivostok 690022, Russia*

Received 26 November 2003; accepted 5 February 2004

Abstract

Sedimentary, geochemical and paleontological data, extracted from a sediment core taken from the central Okhotsk Sea, record climatic and sedimentary changes over the past 100 ky. Benthic foraminiferal oxygen isotope record and accelerator mass spectrometry (AMS) ^{14}C data provide the basis for the core age chronology. Planktonic and benthic foraminiferal $\delta^{18}O$ and $\delta^{13}C$ measurements, magnetic susceptibility, ice rafted debris and coarse fraction content, carbonate and organic carbon content, and diatom and pollen spectra show major changes in regional climate, sea surface conditions, ice extent and sedimentary regime, which are correlated with the global glacial–interglacial changes of marine isotope stages (MIS) 1 through 5.3. Regional cooling and intensification of winter sea ice formation during the last glaciation increased the northern shelf surface water density and Sea of Okhotsk Intermediate Water (SOIW) formation. In addition to major Milankovitch-scale changes, lithological, geochemical and paleontological indices also show suborbital oscillations in Okhotsk Sea hydrology, sedimentation and regional climate. These shorter-term oscillations are characterized by coupled maxima in ice rafted debris and sediment coarse fraction (lithodynamic indices, LDI) values and most are associated with cold events involving enhanced winter ice formation and intensification of SOIW and North Pacific intermediate water (NPIW) formation. The terminations of LDI maxima were induced by climate warming and reductions in ice formation, and were accompanied by sharp decreases in planktonic foraminiferal $\delta^{18}O$. During the glacial terminations of MIS 2 and 4, however, the onset of suborbital-scale LDI maxima occurs close to sharp negative $\delta^{18}O$ shifts in planktonic foraminifera ($\delta^{18}Opf$) associated with climate warming. In these special cases, the LDI maxima occurred under warm climate and rising sea levels and did not lead to increases in SOIW or NPIW ventilation.

Keywords: The Okhotsk Sea; Paleoenvironment; Late Pleistocene; Hydrological and lithodynamical oscillations

* Corresponding author. Fax: +7-4232-312573.
E-mail addresses: gorbarenko@poi.dvo.ru (S.A. Gorbarenko), Southon1@llnl.gov (J.R. Southon), lkeigwin@whoi.edu (L.D. Keigwin), evolut@eastnet.febras.ru (M.V. Cherepanova).
[1] Fax: +7-4232-310193.

0031-0182/$ - see front matter © 2004 Elsevier B.V. All rights reserved.
doi:10.1016/j.palaeo.2004.02.013

1. Introduction

The Okhotsk Sea remains one of the least studied high latitude marginal seas. The majority of papers devoted to Okhotsk Sea climate history have presented paleontological (diatom, pollen) or lithological results (Koreneva, 1957; Jouse, 1962; Bezrukov, 1960); only a few have combined geochemical and paleontological records with a valid age model (Morley et al., 1991; Gorbarenko, 1991, 1996; Keigwin, 1998). Although the Okhotsk Sea is very important for understanding past changes in NPIW formation and the history of the East Asian monsoon (Talley and Nagata, 1995; Porter and An, 1995; Keigwin, 1998), detailed information about millennial-scale climate changes during the Late Pleistocene and Holocene is sparse.

Pacific waters flow into the Okhotsk Sea via the northern Kurile Island Straits, follow a cyclonic circulation and flow out through the southern Straits (Fig. 1) (Moroshkon, 1966; Talley and Nagata, 1995). The sea extends far into the NE Asian continent and its harsh climate has much in common with Arctic shelf seas. A Siberian High–Aleutian Low interaction with strong westerly to northwesterly winter winds and low air temperatures near the northern coast favors polynya phenomena accompanied by extensive formation of new sea ice, enhancement of north shelf water density and Shelf Derived Water (SDW) formation (Martin et al., 1998; Wong et al., 1998; Gladyshev et al., 2000). SDW mixes with North Pacific Water flowing into the Okhotsk Sea and forms the SOIW, which plays an important role in the formation of NPIW (Talley, 1991; Wong et al., 1998). Modern fresh water runoff is 0.02 Sv (1 Sv = 10^6 m^3/s), precipitation over the sea contributes 0.03 Sv, and the flux of the warm and salty Soya Current through La Perouse Strait provides 0.5 Sv (Leonov, 1960; Dr. K. Rogachev, Pacific Oceanological Institute, personal communi-

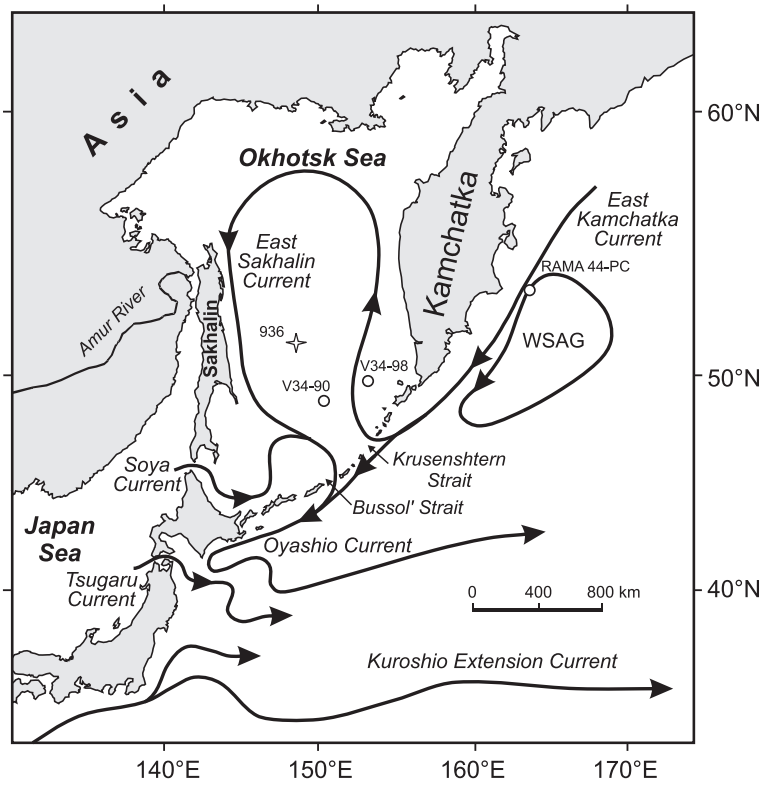

Fig. 1. Okhotsk Sea core locations. Surface water circulation according to Talley and Nagata (1995). WSAG—west subarctic gyre.

cation). This pattern of inflow produces strong salinity and density gradients in the surface water, with salinities of 31‰ in the north and 32‰ in the southeast. A permanent subsurface layer, with a temperature minimum close to freezing point at depths of 50–80 m, is formed during winter. A maximum temperature layer (2–3 °C) is located at 800–1300 m. Temperatures drop gradually in the lower water column, reaching 1.8 °C near the bottom.

As a result of his comprehensive studies of Okhotsk Sea sediments, Bezrukov (1960) inferred three main sources of lithic input to the sea bottom: suspended material from surrounding land carried by runoff, wave erosion of shoreline rocks, and volcanic activity of the Kurile Islands and the Kamchatka Peninsula. Amur River water (63.3% of total runoff) delivers the main part of the terrigenous silt and clay to the sea. Sea ice erosion of the shore and shallow shelf also plays a significant role in the modern sedimentation. Very low winter air temperatures on the north coast favor ice formation and freezing of terrigenous material at low tide. During high tide, the ice and associated sediment floats to the surface and is moved offshore by the prevailing winter winds and surface water circulation (Lisitzin, 1994). During summer, ice melting discharges this ice rafted debris (IRD) that accumulates on the Okhotsk Sea bottom (Lisitzin, 1994).

Here we present well-dated lithological, geochemical, diatom and pollen records from sediment core 936 recovered from the central Okhotsk Sea. From these data sets we infer major changes during the last glacial in sea ice formation, IRD accumulation, and SDW formation. These combined isotopic, geochemical, paleontological and lithological records also show evidence for climatic, environmental and sedimentological oscillations in the Okhotsk Sea on suborbital time scales.

2. Materials, methods and age model

Gravity core 936 was recovered from the relatively flat central part of the Okhotsk Sea (51°00.9′ N, 148°18.8′ E, sea water depth 1305 m) during R/V Akademik Aleksandr Nesmeyanov cruise #25 (1993) (Fig. 1). Shipboard observations identified several lithological units: 0–95 cm—diatomaceous clay, 95–120 cm—transitional silty clay, 120–158 cm—foraminifera-bearing silty clay, 158–275 cm—terrigenous silt with sand, 275–460 cm—terrigenous silty clay, 460–520 cm—terrigenous silty clay with sand, and 520–699 cm—terrigenous silty clay. The sediments were sampled at 3 to 5 cm intervals, with most lithological, geochemical and paleontological analyses being carried out every 5 cm, corresponding to an average temporal interval of 0.7 ky. The isotope analyses in the interval 450–697 cm were conducted every 10 cm.

$CaCO_3$ and total organic carbon content (TOC) were measured by coulometry using an AN-7529 analyser (Gorbarenko et al., 1998). The sediment coarse fraction (>150 μm) was separated and calculated as the weight percent of dry bulk sediment (denoted as CF′). Because the 140 cm^2 cross section of the studied core may be too small to provide representative dropstone fluxes, we also calculated the weight percent of the coarse fraction with pebbles >2000 μm removed (denoted as CF). The numbers of IRD grains in the >150 μm fraction were calculated per gram of dry bulk sediments (without pebbles), based on samples of more than 500 grains.

Oxygen and carbon isotopes in planktonic and benthic foraminifera (δ^{18}Opf, δ^{18}Obf, δ^{13}Cpf, δ^{13}Cbf) were measured on a modified VG mass spectrometer according to previously described methods (Keigwin, 1998). Conversion to the PDB standard is based on analyses of standard NBS-19. The analyses were performed on the benthic species *Uvigerina auberiana* from the 250–350 μm fraction and on the planktonic species *Neogloboquadrina pachyderma* sinistral (s) from the 125–250 μm fraction.

Preparation of samples for diatom analysis and diatom abundance measurement was carried out following the methodology established by Jouse (1962, 1974). In addition to the frequency of more abundant diatom species, we also calculated the pooled frequencies of more representative oceanic and neritic species. The species *Thalassiothrix longissima*, *Thalassiothrix angulata*, *Rhizosolenia hebetata*, *Thalassiothrix eccentrica* and *Neodenticula seminae* were included in the oceanic group with equal statistical weighting. *Bacterosira fragilis*, *Thalassiothrix gravida* (sea ice-edge species) and *Thalassiothrix kryophila* (sea ice dweller) were included in the neritic group, also with

equal statistical weighting. We also estimated diatom paleotemperature (Td) according to (Kanaya and Koizumi, 1966):

$$Td = cw/(cw + cc),$$

where cw is the frequency of relative warm-water species: *Thalassiosira nitzschioides*, *Coscinodiscus radiatus*, *Coscinodiscus perforatus*, *Actonocyclus divisus*, *Th. angulata*, *Stephanopyxis nipponica*, *Thalassiosira pacifica*, *Coscinodiscus asteromphalus*, *Thalassiosira oestrupii*, *Thalassiosira leptopus* and *Stellarima stellaris*; and cc: is the frequency of cold-water species *B. fragilis*, *Th. gravida*, *Thalassiosira nordenskioeldii*, *Th. kryophila*, *Thalassiosira hyalina*, *Nitzschia cylindra*, *Nitzschia grunowii*, *Coscinodiscus oculus-iridis* and *Actonocyclus ochotensis*.

Preparation for pollen analyses followed standard procedures, with 10% KOH treatment and subsequent separation by heavy liquid (Pokrovsky, 1950). Tree-shrub pollen, herb pollen and spore groups were calculated as fractions of the total pollen and spore assemblages, and species percentages inside each group were calculated whenever the group sum exceeded 100 grains. The general qualitative climatic curve was drawn using Tp: the ratio of the frequency of moderate-warm taxa: *Abies*, *Picea*, *Quercus* and other broadleaved (*Ulmus*, *Juglans*, *Corylus fraxinus*, *Carpinus*, *Aralia*, *Tilia*) to the sum of frequencies of moderate-warm plus cold taxa: shrub forms of *Betula* and *Alnaster*. The diatom and pollen coefficients Td and Tp may serve as relative and qualitative indicator of the sea surface and near-land air temperature changes.

N. pachyderma (s.) and *Uv. auberiana* foraminifera from fractions 125–250 and 250–350 μm, respectively, were dated by accelerator mass spectrometry (AMS) at Lawrence Livermore National Laboratory.

The age model for core 936 was constructed using benthic foraminiferal oxygen isotope record, with marine isotope stage (MIS) boundaries according to Martinson et al. (1987), plus AMS ^{14}C dating (Tables 1 and 2; Figs. 2 and 3) and lithology. The preliminary MIS 1 through 5 isotope stratigraphy was supported by correlations with diatom and pollen paleoclimate data (Figs. 4 and 5).

It is possible to place the MIS 2/3 boundary at intervals 275 or 295 cm based on changes in the δ^{18}Obf curve (Fig. 2). The variability in the diatom and pollen species spectra allows us to assign the main changes in surface water condition and surrounding land climate to 275 and 295 cm, respectively (Figs. 4 and 5). Taking in the mind these results, AMS dating and lithology changes we put the MIS 2/3 boundary at 275 cm with ^{14}C age 24 (28.21 cal) ky (Martinson et al., 1987).

All measured radiocarbon ages have been corrected for the Okhotsk Sea surface water reservoir age of 1 ky (JS and SG, unpublished data). The sediments show large changes in $CaCO_3$ content in the upper 170 cm, and some AMS dates have been omitted from the age model because the effects of bioturbation, abundance and dissolution of foraminifera can significantly bias the measured ^{14}C ages (Broecker et al., 1988; Peng and Broecker, 1992).

In the upper core section, we prefer to use ^{14}C data from carbonate peaks. For example, the date of 9.43 ky at 135 cm was rejected because it lies in a valley between two carbonate peaks. The ^{14}C dates at 80 and 91 cm were omitted for a similar reason. The pronounced melt water pulse (MWP) 1A, visible in the δ^{18}Opf record (interval 165 cm) and with a known radiocarbon age of 12.5 ky (Fairbanks, 1989), allows us to rely on more relevant data in the vicinity (at depth 155 cm).

The age difference between coexisting benthic and planktonic foraminifera is usually used to infer the rate of water ventilation in the basin and is an important paleoceanographic proxy (Broecker et al., 1984). These (B-P) age differences (Table 2) in core 936 and other Okhotsk Sea cores (JS and SG, unpublished data) ranged from −3.9 ky up to +3.78 ky in older sediments. Negative and large (B-P) values are due to the influence of bioturbation and dissolution effects in the Okhotsk Sea sediment (Broecker et al., 1988; Peng and Broecker, 1992). *Uv. auberana*, being an infaunal benthic species, may also use the altered pore water dissolved CO_2. Our preliminary assessment is that the (B-P) age difference in this basin is constant through time and is equal to 0.8 ky at 1300 m (based on more reliable Holocene data) (JS and SG, unpublished data). Therefore, in cases of both foraminifera age measurements in one interval, we take the average age, with surface and bottom water reservoir ages equal 1.0 and 1.8 ky, respectively. Constant linear

Table 1
Oxygen and carbon isotopes in *N. pachyderma* s. δ^{18}O N.p, δ^{13}C N.p., ‰ to PDB.), *U. auberiana* (δ^{18}O Uv., δ^{13}C Uv., ‰ to PDB standard), carbonate calcium and organic carbon content (weight %), ice rafted debris (IRD, grain number per gram dry sediment), magnetic susceptibility (MS, CGSM × 10^{-6}), wt.% fraction >150 μm (without and with pebbles) in core 936 through depth

Depth (cm)	δ^{18}C	δ^{13}C	δ^{18}C	δ^{13}C	$CaCO_3$	Corg	IRD	MS	fr>150 μ, (CF)	fr>150 μ(CF′)
	N. p. ‰	*N. p.* ‰	*Uv.aub.* ‰	*Uv.aub.* ‰	wt.%	wt.%	#grain/ 1 g sed	CGSM × 10^{-6}	without pebbles, %	with pebbles, %
0	2.16	0.667	3.199	−0.885	2.5	1.7	94.8		0.456	0.456
5	2.132	0.726			2.67	1.48	257.0		0.622	1.750
10	2.186	0.87	3.02	−0.919	2.83	1.66	100.0	6	0.300	0.300
15	2.208	0.762			2	1.56	138.7	6	0.365	0.365
20	2.309	0.78	3.18	−1.242	2.92	1.55	137.9	6	0.384	0.384
25	1.965	0.637			3.58	1.47	193.5	7	0.466	1.339
30	2.006	0.96	3.199	−0.687	3.92	1.33	139.6	7	0.442	0.442
35	2.165	0.751			3.08	1.23	120.8	7	0.381	0.381
40	1.936	0.926	3.065	−0.898	3.08	1.63	311.0	7	0.559	0.559
45	2.306	0.536			2.75	1.37	190.2	8	0.500	2.330
50	2.416	0.741	3.112	−0.806	3.17	1.82	249.2	8	0.687	0.687
55	1.842	0.685			3.33	1.6	339.2	8	0.751	0.953
60	2.22	0.822	3.185	−0.762	3.67	1.56	194.5	8	0.619	0.619
65	1.932	0.752			3.67	1.86	128.0	10	0.506	0.506
70	1.981	0.694	3.179	−0.763	4	1.92	287.0	11	0.684	2.109
75	1.873	0.921			5	1.3	777.0	12	1.497	1.497
80	2.51	0.516	3.231	−0.776	4.33	1.48	901.0	14	1.610	7.852
85	2.534	0.647			3.67	1.76	792.0	14	1.867	2.123
90	2.64	0.436	3.339	−1.288	3.58	1.57	920.0	15	1.518	1.518
95	2.454	0.629			3.08	1.63	1346.0	18	1.932	1.932
100	2.349	0.35	3.387	−1.602	2.5	1.4	1351.0	21	1.831	2.375
105	2.838	0.231			3.08	1.59	1948.0	26	2.799	2.799
110	2.817	0.342	3.54	−1.821	5	1.8	1198.0	30	2.489	15.738
115	2.567	0.262			6.66	2	1230.0	27	3.079	3.831
120	2.688	0.214	3.496	−1.838	10.25	1.07	1190.0	24	3.455	3.455
125	3.14	−0.082			12.5	2.2	1427.0	27	4.698	4.698
130	2.936	0.24	3.632	−1.841	18.33	2.1	1289.0	29	6.305	6.305
135	2.823	0.073			17.49	2.3	1629.0	32	5.391	15.934
140	3.117	0.072	4.321	−0.856	3.58	1	2111.0	36	2.707	2.707
145	2.993	0.021			8.75	1.45	2513.0	39	4.235	4.235
150	2.931	0.089			11.83	1.78	4696.0	48	5.793	5.916
155	3.091	0.166			10	1.7	4490.0	51	5.335	5.776
160	2.862	0.216	4.408	−0.626	1	0.68	4596.0	55	7.131	8.719
165	2.745	0.26			0.67	0.52	3726.0	77	5.015	5.015
170	3.01	−0.104	4.29	−0.41	0.83	0.5	3430.0	73	4.595	4.595
175	3.046	0.132			1.83	0.58	3930.0	71	4.687	4.687
180	3.26	−0.547	4.648	−0.581	1.08	0.57	3578.0	59	3.808	4.213
185	3.39	−0.15			0.83	0.65	3814.0	59	3.993	4.384
190	3.054	−0.096	4.254	−0.59	1	0.78	3246.0	53	4.454	6.565
195	3.166	−0.226			1.25	0.85	3718.0	50	4.172	4.339
200	3.117	−0.398	4.717	−0.641	1.5	0.82	3562.0	51	4.473	5.320
205	3.47	−0.549	4.724	−0.7	1.58	0.61	4987.0	56	4.893	4.893
210	3.561	−0.479	4.73	−0.668	2.33	1.22		54	4.518	4.518
215	3.528	−0.441			2.08	0.85	4683.0	59	5.384	5.868
220	3.65	−0.815	4.705	−0.796	2.5	0.7	4052.0	56	5.352	7.474
225	3.491	−0.569			3.17	0.74	3946.0	60	5.743	7.430
230	3.561	−0.57	4.619	−0.739	2.67	0.74	4382.0	57	6.363	6.363
235	3.337	−0.349			3	0.7	5289.0	58	5.914	5.914

(continued on next page)

Table 1 (*continued*)

Depth (cm)	$\delta^{18}C$	$\delta^{13}C$	$\delta^{18}C$	$\delta^{13}C$	$CaCO_3$	Corg	IRD	MS	fr>150 μ, (CF)	fr>150 μ(CF′)
	N. p. ‰	*N. p.* ‰	*Uv.aub.* ‰	*Uv.aub.* ‰	wt.%	wt.%	#grain/ 1 g sed	CGSM × 10^{-6}	without pebbles, %	with pebbles, %
240	3.334	− 0.603	4.631	− 0.648	3.75	0.61	3194.0	82	4.497	7.433
245	3.313	− 0.426			1.33	0.54	3320.0	66	5.465	5.644
250	3.208	− 0.697	4.547	− 0.352	1	0.62	3561.0	56	3.980	4.916
255	2.938	− 0.254			2.5	0.7	2905.0	52	5.163	5.163
260	3.344	− 0.112	4.466	− 0.33	1	0.7	3406.0	51	5.300	6.237
265	3.265	− 0.165			1	0.64	4357.0	52	5.105	5.105
270	3.099	− 0.302	4.509	− 0.691	0.83	0.94	3440.0	44	4.966	9.063
275	3.044	− 0.193			0.83	0.7	3271.0		4.283	4.383
280	2.788	− 0.095	4.484	− 0.253	2.08	1.2	2266.0	47	3.446	3.840
285	2.927	0.221	4.47	− 0.532	0.83	0.66	3333.0	51	3.532	3.917
290	2.871	− 0.289	4.417	− 0.562	0.67	0.58	2614.0	58	3.567	3.567
295	2.782	− 0.154			0.5	0.64	1918.0	59	3.029	3.029
300	2.888	0.343	4.253	− 0.409	1.33	0.4	1490.0	95	2.771	2.771
305	2.717	− 0.083			1.67	0.6	3156.0	34	2.749	28.576
310	3.008	− 0.396	4.494	− 0.607	1.67	0.6	3367.0	41	3.801	3.801
315	2.968	− 0.432			3.17	0.82	1728.0	61	2.938	2.938
320	3.047		4.423	− 0.772	5	0.8	1426.0	27	3.182	3.182
325	3.126	− 0.733			2.83	0.76	2426.0	28	3.290	3.290
330	2.75	0.006	4.091	− 0.89	1.67	0.8	2183.0	32	2.803	12.302
335	2.644	− 0.208	4.262	− 0.435	1.25	0.85	1944.0	44	2.799	2.799
340	2.685	− 0.108	4.091	− 0.723	0.58	0.73	2163.0	34	2.957	2.957
345	2.48	− 0.086			1	0.8	3026.0	41	3.589	3.589
350	3.035	− 0.157	4.129	− 0.575	1.67	0.7	3263.0	21	4.025	4.571
355	2.969	− 0.158			1.67	0.8	3415.0	22	3.411	3.830
360	2.771	− 0.229	4.244	− 0.747	1.67	0.8	2935.0	23	4.519	4.818
365	2.943	− 0.254			1	1.08	2358.0	26	3.563	3.563
370	2.67	− 0.254	3.978	− 1.054	1.25	1.05	1851.0	23	3.426	4.011
375					1.25	1.05		31		
380	2.614	− 0.056	3.942	− 0.85	1.5	0.82	1506.0	43	3.424	3.814
385	2.742	− 0.204			0.83	1	3606.0	31	3.887	4.075
390	2.929	− 0.385	4.127	− 0.562	0.83	0.8	3265.0	25	3.910	4.130
395					2.5	1.1	2116.0	23	2.906	2.906
400	2.834	− 0.253	4.3	− 0.673	2.83	0.66	3364.0	28	4.090	4.264
405			4.148	− 0.894	2.5	1.1	2475.0	30	4.236	4.344
410			4.17	− 0.861	2.25	1.13	2578.0	29	3.971	5.882
415	2.871	− 0.385			2.25	1.37	2510.0	26	4.410	5.228
420	2.513	0.024	4.078	− 0.97	2.5	1.1	2489.0	24	4.306	15.552
425	2.87	− 0.083			1	0.88	2715.0	23	3.543	4.501
430	2.916	− 0.103	4.052	− 0.541	0.83	0.9	3440.0	31	4.705	4.705
435					1	0.98	4068.0	34	5.076	5.076
440	2.725	− 0.26	4.15	− 0.878	0.83	1.1	4293.0	32	4.976	5.816
445	2.627	− 0.201			1	0.88	3125.0	38	5.101	5.282
450	2.744	− 0.602	4.203	− 0.955	0.83	0.8	2427.0	41	3.699	4.138
455					0.67	0.92	3866.0	40	4.188	4.684
460	2.915	0.077	4.136	− 0.805	0.5	0.84	4084.0	48	5.044	5.190
465			4.08	− 0.93	0.5	0.54	4638.0	60	5.630	5.630
470	3.21	− 0.56			0.5	0.64	4166.0	76	4.890	6.466
475							3382.0	74	3.763	3.763
480	2.951	− 0.357	4.086	− 0.612	0.5	0.74	3849.0	83	4.466	4.771
485							2948.0	72	3.776	3.776
490	2.194	− 0.368	4.161	− 1.017	1.5	0.88	4371.0	77	5.463	5.674

Table 1 (*continued*)

Depth (cm)	$\delta^{18}C$	$\delta^{13}C$	$\delta^{18}C$	$\delta^{13}C$	$CaCO_3$	Corg	IRD	MS	fr>150 μ, (CF)	fr>150 μ(CF′)
	N. p. ‰	*N. p.* ‰	*Uv.aub.* ‰	*Uv.aub.* ‰	wt.%	wt.%	#grain/ 1 g sed	CGSM × 10^{-6}	without pebbles, %	with pebbles, %
495							4109.0	81	4.367	4.428
500	2.487	− 0.413	4.172	− 0.865	1.67	0.7	3846.0	100	3.679	7.344
505							2480.0	80	3.246	5.641
510	2.931	− 0.375	4.218	− 0.856	1.33	0.64	2294.0	100	3.040	3.287
515							2306.0	70	3.303	3.303
520	3.294	− 1.531	4.206	− 1.008			3837.0	73	4.225	4.225
525							3474.0	73	3.867	3.867
530	2.933	− 0.125	4.153	− 0.798	1.92	0.77	2828.0	74	3.511	3.511
535							3052.0	62	4.120	19.242
540	2.764	− 0.416	4.362	− 0.737	5	0.8	2776.0	61	3.940	4.061
545							2575.0	61	3.595	3.595
550	2.129	0.053	4.133	− 0.904	1	0.68	2217.0	63	3.211	3.211
555							1421.0	66	2.034	7.806
560	2.299	− 0.115	3.975	− 0.562	1.58	0.71	2468.0	62	3.025	3.025
565							2196.0	34	2.580	6.709
570	2.746	− 0.813	3.972	− 0.744	2.92	0.95	2330.0	30	3.510	4.134
575							1455.0	28	2.130	2.976
580	1.989	0.25	4.119	− 0.666	1	0.88	2072.0	27	2.927	2.927
585							1493.0	25	2.041	2.041
590	2.3	− 0.12	3.847	− 0.688	1	0.88	1899.0	27	2.185	2.185
595							1663.0	25	1.819	1.819
600	2.131	0.13	3.893	− 0.444			2452.0	21	2.778	2.778
605							1521.0	21	1.735	7.007
610	2.831	− 0.326	3.824	− 0.732	2.08	0.95	1160.0	17	1.939	13.201
615							1513.0	16	1.852	1.852
620	2.519	− 0.047	3.719	− 0.794	1.33	1.04	1688.0	15	2.182	2.182
625							1196.0	17	1.370	2.313
630	2.759	− 0.172	3.638	− 0.714	2.5	1.15	1533.0	16	2.622	8.706
635							666.0	29	1.388	1.388
640	2.811	− 0.747	3.654	− 0.961	2.67	0.68	1207.0	15	1.720	1.720
645								51		
650	2.859	− 0.976	3.777	− 0.891	5	0.7	2381.0	41	3.082	3.082
655								29		
660	2.79	− 0.932	3.9	− 0.723	1.25	0.8	2141.0	32	2.265	2.418
665							1832.0	29	3.900	3.900
670	2.336	− 0.096	3.968	− 0.682	1.33	1.04	1068.0	30	1.656	1.656
675							2196.0	27	2.548	2.548
680	1.942	0.157	3.894	− 0.77	1.67	0.9	1317.0	32	1.765	1.765
685							2393.0	30	2.699	2.699
690	2.636	0.518	3.83	− 0.822	1.67	1	4102.0	26	4.331	4.331
695	2.777	0.316					2334.0	22	2.796	5.330
697	1.898	0.278	3.901	− 0.485	1.17	1.06	4155.0	24	3.511	4.246

sedimentation rates between AMS data and MIS boundary ages were assumed.

The Okhotsk Sea's linear sedimentation rate (LSR) pattern is an additional criterion for verifying radiocarbon data. LSR values (Fig. 3b) show moderate accumulation during MIS 4, 5.1, 5.2 and 5.3 (6 cm/ky). Sedimentation rates were lowest during MIS 3 (high LSR values near the top of this stage reflect deposition of the K2 tephra (Gorbarenko et al., 2002a,b). Accumulation during glacial stage 2 was rapid with maxima during the transition from MIS 2 to 1 (9–14.5 cm/ky). This is typical for the Okhotsk Sea,

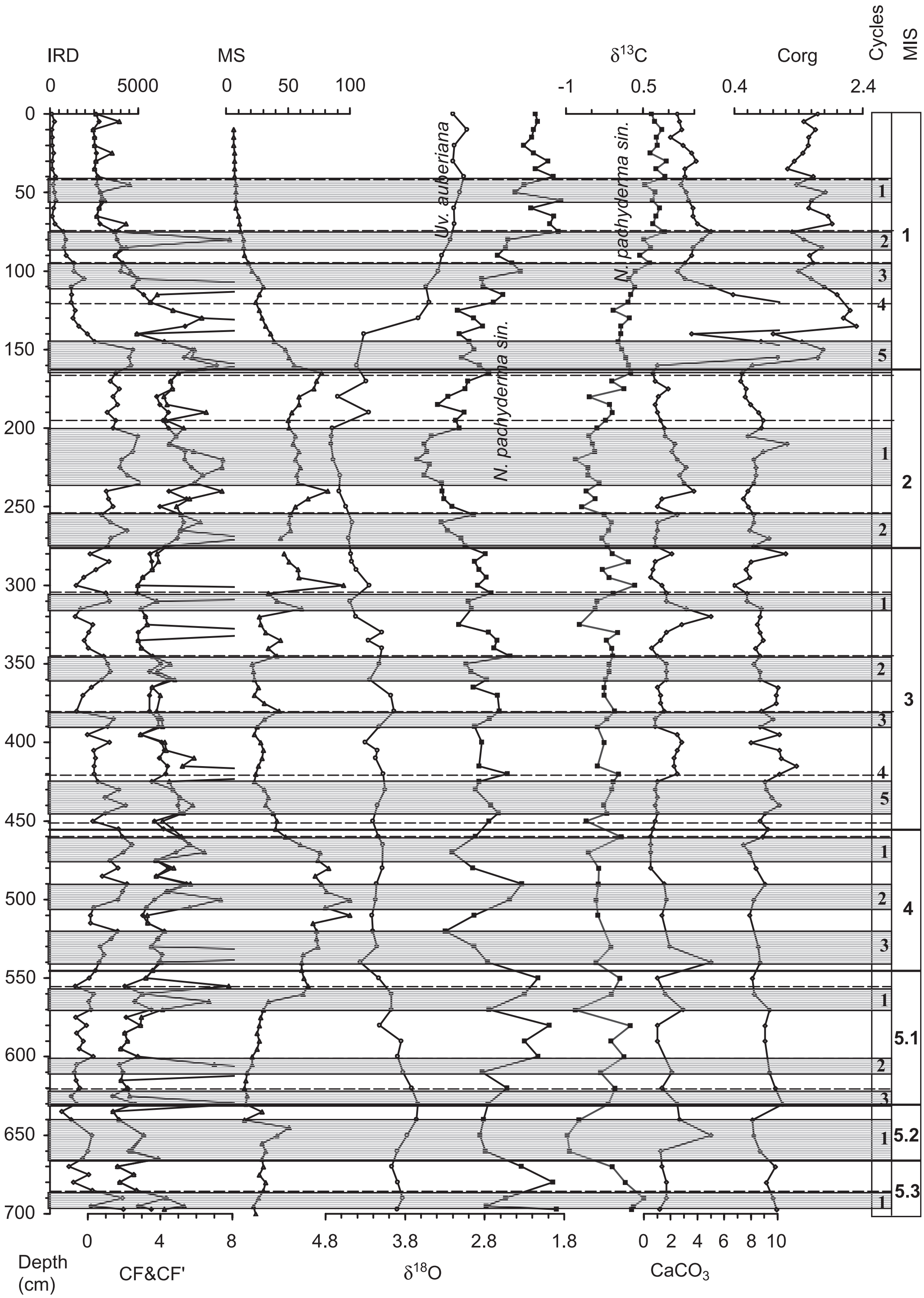
IRD
MS
δ13C
Corg
Cycles
MIS
Uv. auberiana
N. pachyderma sin.
N. pachyderma sin.
Depth (cm)
CF&CF'
δ18O
CaCO3

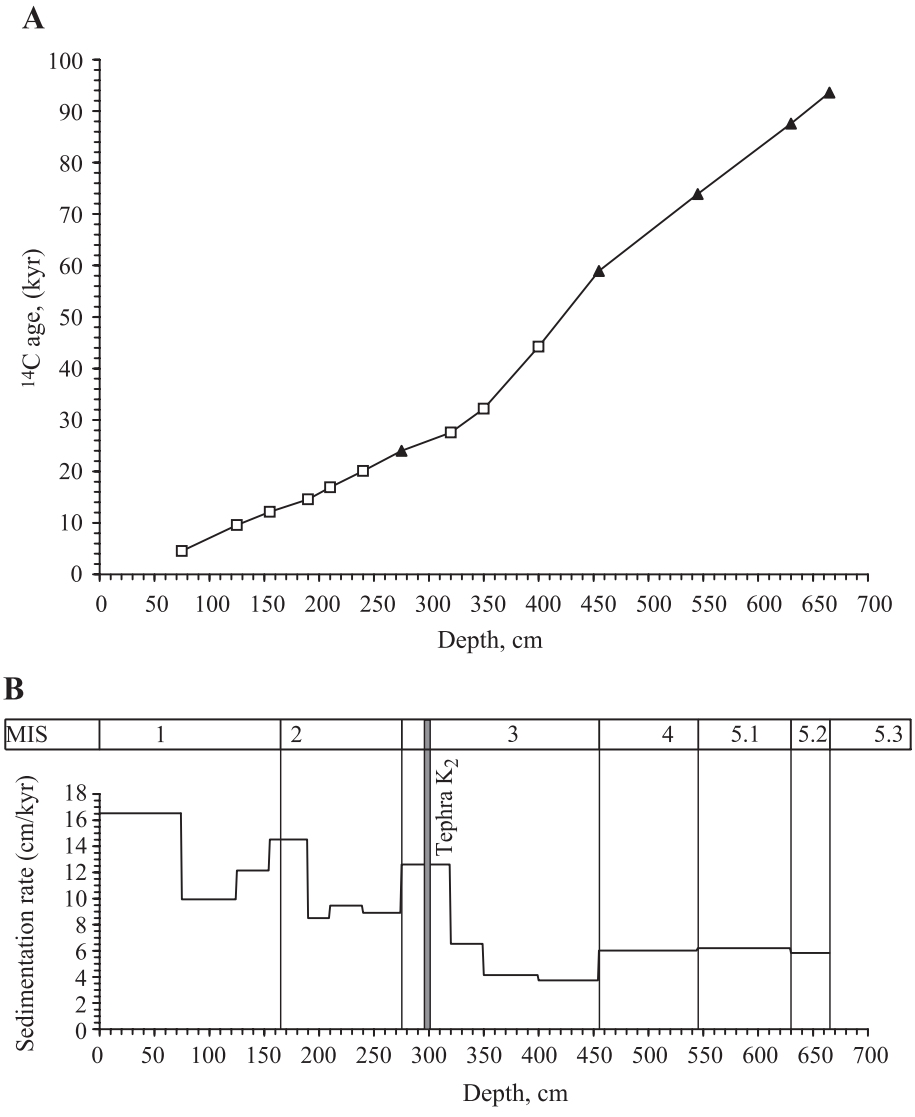

Fig. 3. (A) Core 936 depth (cm) vs. AMS ^{14}C age (ky) and MIS boundary age: open squares, AMS data used in age model (see text); triangles, MIS boundary ages according to Martinson et al. (1987). (B) Linear sedimentation rate (cm/ky) according to the age model. Note that the high sedimentation rate for the end of MIS 3 is induced by the K_2 tephra accumulation.

which is characterized by substantial changes in terrigenous input during the last glacial and deglacial times. The LSR maximum in the upper part of MIS 1 (up to 16 cm/ky) is associated with a major rise in biogenic opal productivity (diatom) since 5 ky BP (Gorbarenko et al., 2002a,b).

We converted ^{14}C ages to calendar ages using a Holocene polynomial up to 10 ky and a Glacial one

Fig. 2. Records of ice rafted debris (IRD) (grain number/gram of dry sediment), coarse sediment fraction >150 μm (wt.%) without pebbles (CF, thick line) and with pebbles (CF′, thin line), magnetic susceptibility (CGSM × 10^{-6}), δ^{18}O of *U. auberiana* and δ^{18}O and δ^{13}C of *N. pachyderma* s. (in ‰ relative to PDB) and carbonate and organic carbon content (wt.%), all plotted versus depth (cm) in core 936 sediment. The short-term maxima in CF and IRD records are marked by stippled strips and sharp negative δ^{18}pf shift are indicated by dashed lines. The oxygen isotope stages and high frequency oscillations are shown at the right.

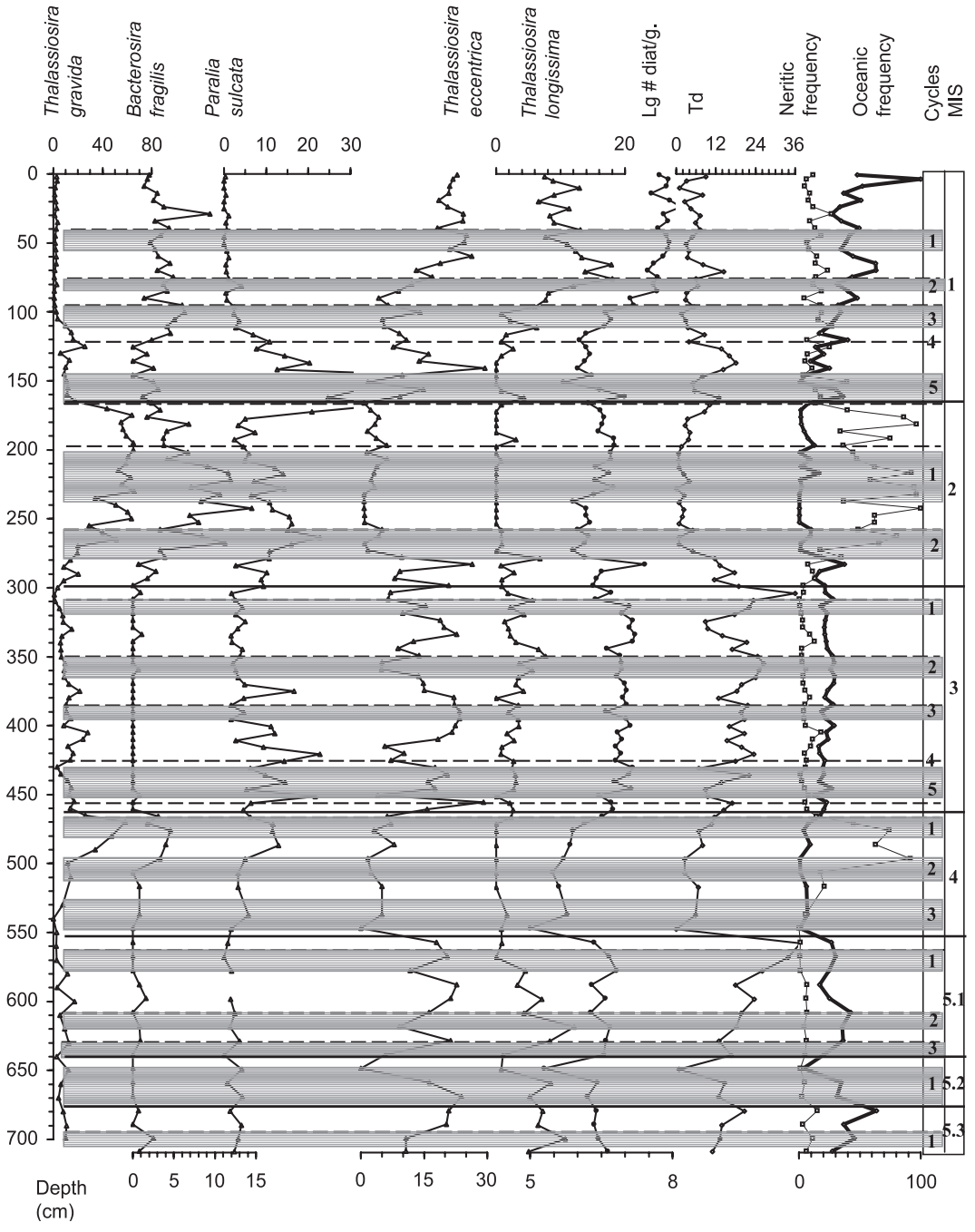

Fig. 4. The frequency (in %) of indicative diatom species *Th. gravida*, *B. fragilis* (neritic species), *P. sulcata*, *Th. eccentrica*, *Th. longissima*, diatom abundance (Lg# diatom/gram of dry bulk sediment) and calculated neritic (open square) and oceanic diatom (bold line) groups frequencies (in %, see text) are shown vs. core 936 depth. The isotope stages and suborbital oscillations are shown as in Fig. 2.

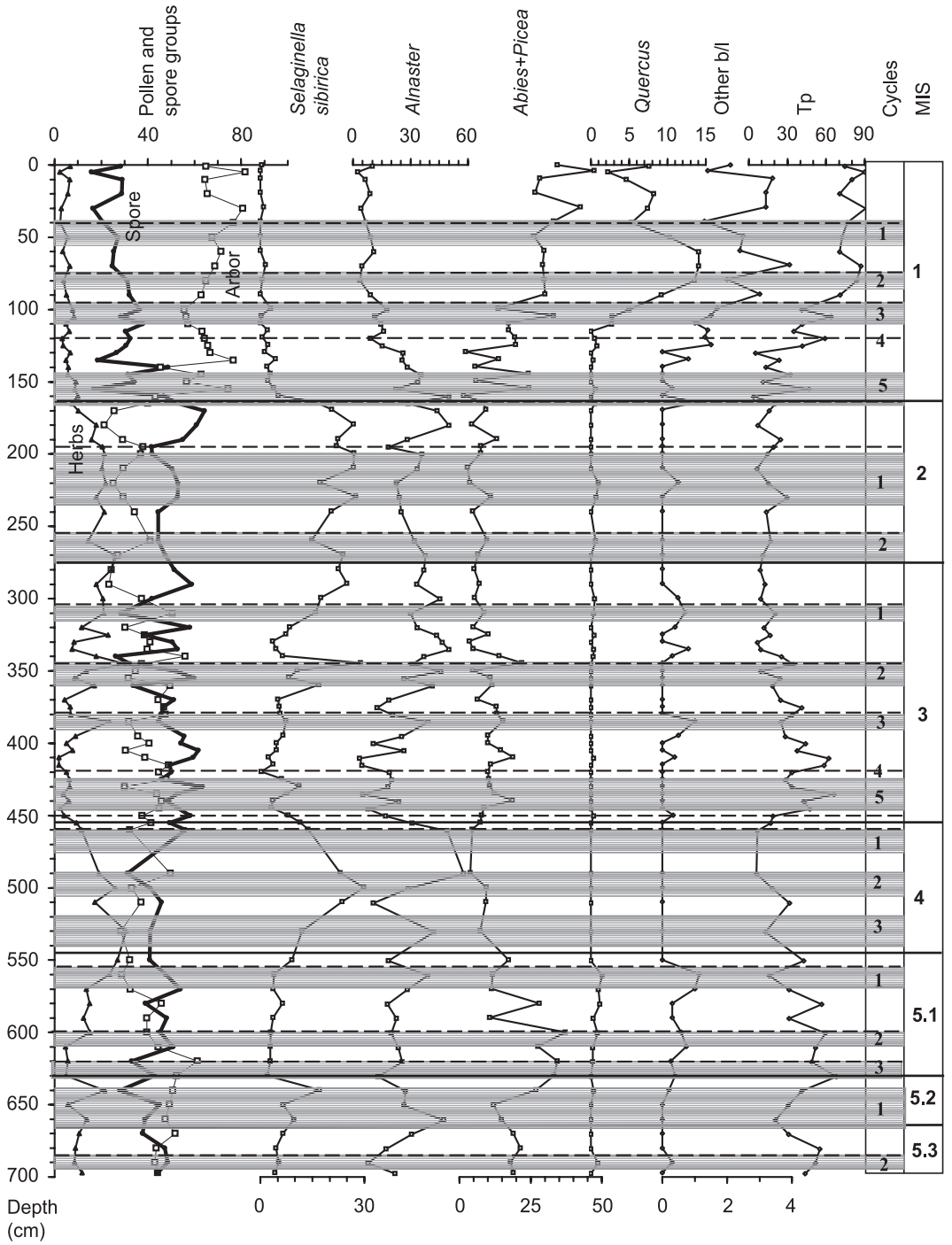

Fig. 5. Changes of herbs, spores and tree-shrub groups in the total pollen assemblages (in %) and warm climate pollen value Tp (%) in core 936. The *Selaginella sibirica*, *Alnaster*, *Abies+Picea*, *Quercus* and other broadleaved species percentages inside each group were calculated whenever the grain sum exceeded 100. The isotope stages and suborbital oscillations are shown as in Fig. 2.

Table 2
AMS ^{14}C data on monospecies planktonic and benthic foraminifera for core 936

Accession Cams#	Depth (cm)	Foram species	AMS ^{14}C age (ky)	Error ($\pm$ ky)	AMS ^{14}C age corrected	B-P foram difference	Age model age ^{14}C/cal ky
55353	75[a]	*N. pach. sin*	5.54	0.05	4.54		4.54/5.14
62181	80	*N. pach. sin*	6.27	0.05	5.27		
53919	90–92	*N. pach. sin*	8.15	0.05	7.15		
56789	120	*N. pach. sin*	10.3	0.05	9.3		
62182	125[a]	*N. pach. sin*	10.57	0.05	9.57		9.57/10.76
47658	135	*N. pach. sin*	10.43	0.05	9.43		
34107	150–152	*N. pach. sin*	13.04	0.07	12.04		
62183	155[a]	*N. pach. sin*	13.14	0.06	12.14		12.14/14.21
55354	190[a]	*N. pach. sin*	15.55	0.08	14.55		14.55/17.12
34109	210–212[a]	*N. pach. sin*	17.53	0.14	16.53		16.90/19.93
56790	230	*N. pach. sin*	19.42	0.11	18.42		
34111	240[a]	*N. pach. sin*	21.76	0.17	20.76		20.07/23.66
55355	255	*N. pach. sin*	20.09	0.15	19.09		
46588	320[a]	*N. pach. sin*	27.12	0.29	26.12		27.57/32.26
55356	350[a]	*N. pach. sin*	33.16	0.66	32.16		32.16/37.35
34112	400[a]	*N. pach. sin*	47.6	4	46.6		44.25/47.56
34108	150–152	*Uvigerina* sp.	14.1	0.07	12.3	1.06	
34110	210–212[a]	*Uvigerina* sp.	19.07	0.11	17.27	1.54	
20033	240–242[a]	*Uvigerina* sp.	21.18	0.1	19.38	− 0.58	
20034	320–322[a]	*Uvigerina* sp.	30.73	0.39	28.93		
46589	320[a]	*Uvigerina* sp.	30.9	0.4	29.1	3.78	
47657	400–402[a]	*Uvigerina* sp.	43.7	1.6	41.9	− 3.9	
20035	650–652	*Uvigerina* sp.	>47.200		>45.400		

All ^{14}C age data measured were corrected by Okhotsk Sea surface and bottom water reservoir age equal minus 1.0 and 1.8 ky, respectively. For radiocarbon-calendar age conversion, see text.

[a] Indicates ^{14}C data used for age model reconstruction (see text).

from 10 ^{14}C ky up to 36 ky (Bard, 1998). After 36 ky, the age difference between calendar and ^{14}C years decreased linearly from a 5.21 ky difference at 36 ^{14}C ky to 0 at 58.96 ky (age of MIS $\leq$boundary).

2.1. Glacial hydrology and sedimentology

Values of MS, IRD and CF in core 936 (Fig. 2; Table 1) and other Okhotsk Sea sediments (Gorbarenko et al., 2002a,b) are high in glacial and low in interglacial sediments. During glacial periods, iceberg discharge from coastal glaciers represents another potential source of lithic input into the sea interior, but available geomorphological results do not show sufficiently increased glacier volume to allow land glaciers to have reached sea level (Braitseva and Melekestsev, 1974; Ananjev et al., 1993). Therefore, sea ice probably remained the main carrier of coarse terrigenous material from land to the sea bottom during glacial times. The glacial climate at high latitudes was characterized by an enhanced winter Siberian High (COHMAP Members, 1988; Porter and An, 1995) and increased in westerly and northwesterly winter winds in the Okhotsk Sea. The extreme cold glacial climate (Atlas, 1992) and strengthening of the winter Siberian High favored increased ice formation on the north shelf and its loading by coarse lithic particles, consistent with IRD, CF results, and silty sediment accumulation. IRD records from core 936 (Fig. 2) and additional Okhotsk Sea cores show that the accumulation rate of IRD in sea during MIS 2 was several times greater than modern (Gorbarenko et al., 2001). Therefore, during glacial times, much marine ice loaded by terrigenous material was formed on the north shelf and extended far across the basin surface in winter. This rise in sea ice formation would have increased the northern shelf water density due to salt rejection and therefore could have led to denser SDW, SOIW and NPIW

formation. Although Shiga and Koizumi (2000) concluded that the western Okhotsk Sea was permanently covered by sea ice during glaciation, IRD data from cores recovered from different parts of the sea argue that most of the glacial Okhotsk Sea was not covered by permanent ice (Gorbarenko et al., 2001, 2003). Increased brine rejection, coupled with seasonally open waters and greater storminess and mixing, may have set the stage for volumetric increases in these water masses.

The Holocene–LGM shift in δ^{18}Obf of 1.5‰ is reduced to 0.2‰ after correction by 1.3‰ for the global ice volume effect (Fairbanks, 1989), suggesting insignificant changes in the bottom water conditions over this time period. However, the benthic foraminifera assemblages present in cores V34-90 and V34-98 (locations in Fig. 1) during glacials show that bottom water temperatures were close to or below zero (Gorbarenko et al., 2002a,b). A temperature drop from 1.8 °C today to zero should have increased glacial δ^{18}Obf by 0.4–0.5‰ (Shackleton, 1974). In order to reconcile the observed minimal glacial shift in δ^{18}Obf (0.2‰) with the assemblage data thus requires an inflow of cold and dense water with low δ^{18}O. This can be supplied only from the north shelf during winter sea ice formation, which occurs without isotope fractionation (Craig and Gordon, 1965). Thus, the combined δ^{18}Obf and benthic foraminifera species studies are consistent with observed lithodynamic records, indicating glacial stage enhancement of sea ice formation on the north shelf and strengthening of SDW, SOIW and NPIW formation.

As with δ^{18}Obf, the Holocene–LGM δ^{18}Opf shift of −1.4‰ is small compared to the LGM ice volume effect of 1.3‰ (Fairbanks, 1989). The glacial summer surface temperature was 2–4 °C lower than modern ones in the studied area (CLIMAP, 1981). Ecological evidence indicates that *N. pachyderma* s. dominantly calcifies its shells near the main halocline (depth 100–150 m) (Bauch et al., 1997) or just above the subsurface temperature minimum (20–40 m) (Alderman, 1996). Therefore the glacial temperature effect on δ^{18}Opf probably did not exceed 0.2–0.3‰ This implies that changes in δ^{18}O and salinity of the surface water in the sea were minor and supports our hypothesized hydrologic changes on the north shelf and strengthening of the SDW and SOIW formation.

Planktonic δ^{13}C difference between Holocene (0.75‰) and MIS 2 (−0.1‰ to 0.5‰) indicates that Late Holocene δ^{13}C in dissolved inorganic carbon (DIC) in surface water at the 936 core site was much lower (about 1.1‰) during the glacial. Other Okhotsk Sea cores from further to the southeast (Fig. 1) (Gorbarenko, 1996; Keigwin, 1998; Gorbarenko et al., 1998) reveal interglacial–glacial δ^{13}Cpf decreases ranging from 0.2‰ to 0.9‰, with the smallest change in core V34-98 which is most strongly influenced by Pacific water inflow. The high 936 LGM–Holocene δ^{13}Cpf shift is close to carbon isotope shifts observed in the surface waters of the Southern Ocean and at high northern latitudes (0.3–0.9‰) (Charles and Fairbanks, 1992).

Elevated North Pacific productivity (Sancetta, 1992) induced δ^{13}C enrichment in surface waters, offsetting the whole ocean drop (Hofmann et al., 1999). Contrary to the North Pacific productivity change pattern, the Okhotsk Sea TOC records of 936 and other cores indicate lower glacial productivity compared with warmer periods of MIS 1, 3 and 5 (Gorbarenko, 1996; Gorbarenko et al., 2002a,b). This difference between open ocean and marginal seas can be accounted for by greater ice cover in the Okhotsk Sea (in the Bering Sea as well) than in the North Pacific during glacial periods. A large Okhotsk Sea drop in the δ^{13}C of surface DIC also suggests that a strong regional biogeochemical fractionation mechanism was present. This additional reduction in glacial Okhotsk Sea surface DIC δ^{13}C may be attributable to a large reduction in air–sea gas exchange due to the increased sea ice cover shown by the IRD data. Winter ice cover in high latitude basins probably has a crucial role in regulating sea–air gas exchange, since the winter exchange rates would otherwise be very high due to low temperatures and high wind speeds. Lynch-Stieglitz et al. (1995) shows that high sea–air exchange shifts the δ^{13}C of surface DIC by up to 1.5‰ in the modern North Pacific.

The high abundance of the cold water neritic taxa *Th. gravida* and *B. fragilis* and low percentages of the oceanic group points to the presence of marine ice throughout much of the year during MIS 2 and late Stage 4 (Fig. 4). Based on study of diatom assemblages from the Okhotsk Sea surface and core sediments, Jouse (1962) has established that the dominance of neritic species that live near the ice edge during ice melting, over oceanic group, indicates a strong sea ice

influence in the central basin during glacial conditions. The responses of neritic and oceanic diatom groups to climatic and environmental changes observed in core 936 are in line with IRD and other results and consistent with Jouse's conclusion (1962) thus providing a complementary paleoceanographic proxy for ice influence in high latitude basins. The early part of the MIS 4 is characterized by unusual low frequency of both neritic and oceanic groups and dominance by specific diatom species. Both colder climate periods MIS 2 and 4 are characterized by very low common diatom abundance (Fig. 4).

Pollen spectra indicate a higher percentage of herb and spore groups and a lower percentage of arboreal pollen in the total composition during cold MIS 2 and 4 as compared to warm MIS 1, 3 and 5 (Fig. 5). More representative arboreal species *Abies* and *Picea* prevailed during warm MIS 1 and 5 and to a lesser extent also in MIS 3. The species spectra, the total pollen-spore composition and the low Tp coefficient values in MIS 2 and 4 (Fig. 5) point to a very cold and dry climate in the area around Okhotsk during glacials with the most severe conditions occurring during MIS 2. This conclusion agrees with earlier pollen results from NE Asia, Okhotsk Sea sediments and Hokkaido Island (Atlas, 1992; Koreneva, 1957; Tsukada, 1986). These pollen data confirm earlier CLIMAP (1981) and regional paleogeographical results (Atlas, 1992; Ananjev et al., 1993) indicating that the LGM climate in northeastern Asia was both colder and drier than at present.

2.2. High-frequency environmental oscillations

In addition to the Earth orbitally forced long-term changes, the core 936 geochemistry, lithology and paleontology results show the presence of suborbital oscillations (Figs. 2, 4 and 5). In order to evaluate the connection of different core 936 proxies, we calculated a cluster dendrogram based on the averaged stepwise correlation values of sediment properties (CF, IRD, MS), geochemistry (δ^{18}Opf, δ^{18}Obf, δ^{13}Cpf, δ^{13}Cbf, TOC and $CaCO_3$ % content), and paleontological parameters (diatom abundance in sediment (DT), % of calculated oceanic diatom group (OCD) and pollen climate coefficient Tp (Fig. 6). The

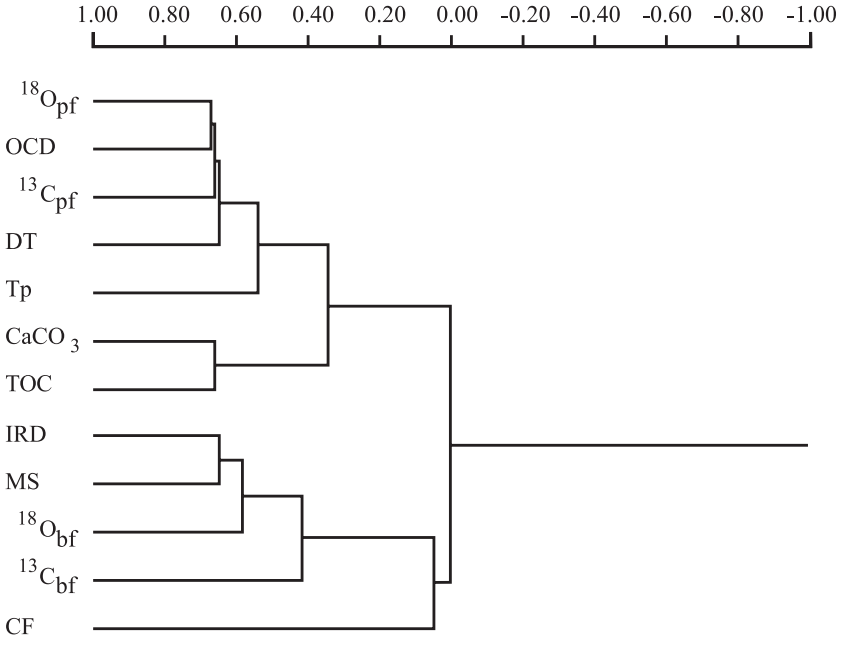

Fig. 6. Cluster diagram plotted on the base of the correlation coefficient matrix for variables: wt.% of the >150 μm fraction (CF), IRD and magnetic susceptibility (MS), δ^{18}pf, δ^{18}Obf, δ^{13}Cpf, δ^{13}Cbf, TOC and $CaCO_3$ content, abundance of diatom frustules (DT) and calculated ocean diatom group frequency (OCD) and warm climate pollen coefficient Tp value of core 936. All values were preliminary centered and normalized by middle-square deviation. The *x*-axis shows the correlation coefficient for these variables.

visual correlation of these proxies and the results of the cluster dendrogram allow us to separate two major groups of parameters.

The first group includes IRD, MS and CF plus geochemistry of the benthic foraminifera (δ^{18}Obf and δ^{13}Cbf) (Fig. 2). In this group we concentrate on the first three indices (IRD, MS and CF) which characterize the lithophysical properties of sediments and influenced by the lithic sedimentation in the basin (denoted as lithodynamic indices (LDI). Oscillations in LDI marked as "L" are traced by maxima in IRD and CF mainly transported in the open sea by sea ice (Fig. 2, stippled strips; Table 3). Correlation of IRD and CF with MS is probably less pronounced (Fig. 2) since the MS of core 936 is defined more by a silty fraction than by fine sand (Gorbarenko et al., 2002a,b). The occurrence of dropstones in the sediment (Fig. 2, peaks in curve CF′) usually occurs synchronously with IRD and CF maxima and confirms the increase in coarse lithic accumulation

Table 3
Location and age of high-frequency surface environmental (SEI) and lithodynamic (LDI) indices (S and L) oscillations are indicated according to multiproxy records of core 936

SEI # (S), LDI # (L)	Interval, cm	^{14}C age, ky	Cal age, ky	Surface environment	Land climate
S1/1	40	2.42	2.46	w	w
L1/1	40–55	2.42–3.33	2.46–3.62	c	c?
S1/2	75	4.54	5.14	w	w
L1/2	75–85	4.54–5.55	5.14–6.32	c?	w?
S1/3	95	6.55	7.41	w	w
L1/3	95–110	6.55–8.06	7.41–8.98	c?	c?
S1/4	120	9.07	10.12	w	w
L′1/5	165–145	12.83–11.28	15.04–13.16	w	w
S′1/5	165	12.83	15.04	w	w
S2/1	195	15.14	17.83	w	w
L2/1	200–235	15.72–19.54	18.53–23.45	c	c
S2/2	255	21.69	25.54	w	w?
L2/2	255–275	21.69–24.0	25.54–28.21	c	c
S3/1	305	26.63	31.2	w	c?
L3/1	305–315	26.63–27.26	31.2–31.91	c?	w?
S3/2	345	31.4	36.51	w?	w
L3/2	345–360	31.4–34.58	36.51–39.98	w?	c
S3/3	380	39.41	43.81	w	w
L3/3	380–390	39.41–41.83	43.81–45.68	c	c
S3/4	420	49.6	51.7	w?	w
L′3/5	425–445	50.94–56.28	52.7–56.9	?	w
S′3/5	450	57.62	57.92	w	w
S4/1	460	59.79	59.79	w	w?
L4/1	460–475	59.79–62.28	59.79–62.28	c	c
L4/2	490–505	64.77–67.26	64.77–67.26	c	c
L4/3	520–540	69.76–73.08	69.76–73.08	c	c
S5.1/1	555	75.52	75.52	w	w
L5.1/1	555–570	75.52–77.93	75.52–77.93	w?	c?
S5.1/2	600	82.76	82.76	w	w
L5.1/2	600–610	82.76–84.37	82.76–84.37	w?	w?
S5.1/3	620	85.98	85.98	w	c?
L5.1/3	620–630	85.98–87.59	85.98–87.59	w	w
L5.2/1	640–665	89.31–93.58	89.31–93.58	–	–
S5.3/1	685	97	97	w?	w
L5.3/1	685–695	97–98.71	97–98.71	c?	c?

Numerator denotes the MIS number, denominator the S and L oscillation number inside each MIS. Relative changes in the surface water environment and surrounding land climate, which occurred synchronously with these oscillations (warmer, cooler), are shown in line with the diatom and pollen data set, respectively.

′ Cycles demonstrate the reversed oscillation sequences when SEI triggered LDI oscillations (see text).

during these periods. The second tight group combines planktonic foraminifera $\delta^{18}O$ and $\delta^{13}C$ values, the diatom abundance (DT), the oceanic diatom group % (OCD) and the pollen climate coefficient Tp (Fig. 6). The first four factors are mainly defined by surface water geochemistry and productivity and may be called the surface environmental indices (SEI). The oscillations in the SEI are traced by sharp negative shifts in δ^{18}Opf (marked as "S") and are illustrated in Figs. 2, 4 and 5) by dashed lines. Variability in total organic matter (TOC) and $CaCO_3$ content, defined by the productivity and dissolution in sediment, are more isolated on the dendrogram (Fig. 6).

There are significant regularities in the high-frequency oscillations of core 936. The majority of the SEI and LDI oscillations are coupled. In most cases, the S oscillations terminate the longer duration L-oscillations ("normal" Okhotsk Sea cycle) (Fig. 2). However, in cycles that occurred at the terminations of cold MIS 2 and 4, the S oscillations triggered broader LDI maxima (S–L1/5 and S–L3/5 cycles). We denote these as "reverse" cycles. The cycle 5.1/3 occurred at the beginning of the relative warm substage 5.1 may be also accept as "reverse" according to clearly expressed warming of the sea and land at termination of the MIS 5.2 (630 cm, Figs. 4 and 5). High-resolution records are needed to clarify some discordance between the isotopic δ^{18}Opf and δ^{13}Cpf and paleontological evidence during this cycle. Some of the L-oscillations that occurred during cold stages (MIS 4 and 5.2) are not clearly terminated, according to the geochemical and paleontological proxies used in this study. Probably more subtle indicators of high latitude glacial paleoenvironment are needed.

The LDI maxima (IRD and CF) may be forced either by climate cooling with increases in sea ice formation and terrigenous material accumulation (as during the longer orbital changes), or by climate warming accompanied by mountain glacier melting and sea level uplift, which supplied more terrigenous material to the shoreline. The sharp negative shifts in the δ^{18}Opf may be influenced both by surface water warming and by freshening due to increased precipitation or reduced evaporation. Diatom and pollen results based on changes of indicator species, the relationship of oceanic-neritic diatom groups, diatom paleotemperature Td values and the warm climate pollen coefficient Tp, suggest preliminary climate and environment interpretations of the SEI and LDI oscillations (Figs. 2, 4 and 5), dashed lines and stippled strips, respectively; Table 3). Increase abundance of the relative warm diatom and pollen species and their coefficients Td and Tp, respectively, indicate warming on the surface water and surrounding land. Increase of the neritic diatom group (sea ice-edge and ice species) in core 936 is likely influenced by sea ice extent in the sea and usually forced by climate cooling (Jouse, 1962; Gorbarenko et al., 2003).

For "normal" Okhotsk Sea cycles, the maxima in IRD and CF mainly correlate with colder climate and sea surface conditions (Figs. 4 and 5, Table 3). The extreme cold and dry climate of surrounding land enhanced winter sea ice formation and ice cover advance (Kimura and Wakatsuchi, 1999), which led to an increase in IRD and CF accumulation for summer ice melting. As mentioned earlier enhanced winter sea ice formation on the north shelf during L-maxima in turn forced more extensive SDW, SOIW and NPIW ventilation by means of mechanisms similar to modern ones (Kitani, 1973; Talley, 1991; Wong et al., 1998; Gladyshev et al., 2000). The colder and dryer climate for LDI maxima are also consistent with high δ^{18}Opf (Figs. 2, 4 and 5). The negative shifts in δ^{18}Opf, which terminate these LDI maxima, are mostly correlated with warming events in the sea and surrounding land (Table 3). Thus, the linkage of the Okhotsk Sea S–L oscillations with environmental and climate variability is less clearly pronounced for some cycles during relative warm climate periods MIS 3 and 5.1 (S–L 3/1 and 5.1/1 cycles, Table 3).

The onset of the "normal" LDI maxima often coincides with some decrease in the TOC % in sediment that was likely induced by the strengthening in the spatial extent and seasonal duration of ice cover (Fig. 2). The resulting decrease in productivity during the LDI maxima (Fig. 2) tends to decrease the $\delta^{13}C$ of dissolved CO_2 in shallow water. The alternative explanation for the drop in $\delta^{13}C$ of ΣCO_2 is that it is probably associated with the intensity of sea surface–atmosphere CO_2 exchange (Lynch-Stieglitz et al., 1995) due to enhanced sea ice extent and hampered air–sea carbon dioxide exchange. Therefore one may suggest that climate warming and ice extent shrinking, at the end of L-maxima should be accompanied by rising in δ^{13}Cpf as well as by dropping in

δ^{18}Opf. Though the cluster dendrogram demonstrates significant correlation between δ^{18}Opf and δ^{13}Cpf (0.66) (Fig. 6), the sharp positive δ^{13}Cpf shifts at L-maxima termination do not always occur in phase with drop in δ^{18}Opf-S-oscillation (Fig. 2).

According to paleontology results, "reverse" L1/5 and L3/5 cycles at the end of the cold MIS 2 and 4 were initiated by S oscillations (drop in δ^{18}Opf and likely rise in δ^{13}Cpf associated with climate warming. The LDI maxima of these cycles are large (especially the L1/5) and were likely influenced by sea level uplifting and melting of mountain-valley glaciers during warming, leading to increased terrigenous matter input to the shoreline by fluvial fluxes. Synchronous with the L1.5 oscillation, the large TOC and $CaCO_3$ content peaks were likely induced by climate warming and melt water, and terrigenous material input (12.8 ^{14}C or 15.04 cal ky). Accelerated sea level rise coeval with global MWP 1A (Fairbanks, 1989) initiated the productivity blooms in the NW Pacific, Okhotsk, and Bering Seas (Keigwin et al., 1992; Gorbarenko, 1996; Gorbarenko et al., 2002a,b). This probably resulted in intensive Fe delivery into basins together with terrigenous material (LSR peak at Fig. 3b), and in an increase in N_2 fixation and nutrient limited nitrate content in water (Falkovski et al., 1998). Pollen results indicate a moderate climate warming for the S 1/5 oscillation (MWP 1A) and a major climate warming after the cold Younger Dryas event, during the S 1/4 oscillation coeval with MWP 1B (Table 3). Therefore, the large negative δ^{18}Opf shift in S 1/5 oscillation (MWP 1A) was probably influenced more by lower surface water salinity than by a higher temperature (Figs. 4 and 5). Glacial sediments in core 936 have very low carbonate content with a series of less prominent spikes during MIS 2–5 in the $CaCO_3$ content (Fig. 2). Our unpublished data suggest that small carbonate oscillations may be typical for the far NW Pacific and its marginal seas.

Based on a study of the distribution of diatom assemblages in the surface sediments of the far NW Pacific and its marginal seas, Jouse (1962) and Sancetta (1981) describe the *Paralia* (former *Melosira*) *sulcata* as a typical shelf-water, low salinity diatom species. The large spike in *P. sulcata*'s relative frequency (up to 57%) during the L 1/5 oscillation in core 936 (Fig. 4) allows us to suggest that this species is a sensitive indicator of surface water freshening in the open Okhotsk Sea and likely in the Bering Sea and far NW Pacific as well. There are significant changes in *P. sulcata* frequency during MIS 2, 3 and 4, mostly correlated with observed high-frequency oscillations. The causes of these and other suborbital oscillations in the Okhotsk Sea and the linkages between regional and global short-term climate changes remain open to question. Similar oscillations have been extensively studied in the North Atlantic following the discovery of the Dansgaard–Oeschger interstadials in Greenland ice cores (Dansgaard et al., 1993), Heinrich events (Heinrich, 1988) and Bond cycles (Bond et al., 1993) in North Atlantic sediments.

The Okhotsk LDI and SEI climate responses are more closely tied to the cycles observed in the NE Pacific at Site 893A in the Santa Barbara Basin (Hendy and Kennett, 2000). The LDI maxima and δ^{18}Opf high, observed during the "normal" Okhotsk Sea L oscillations, correlate with high δ^{18}Opf values in the stadial sediments of Site 893A (Fig. 7). The strengthening of SDW and SOIW formation in the Okhotsk Sea during these periods probably increased NPIW formation and led to better North Pacific ventilation and hence to the presence of bioturbated sediments in the Santa Barbara Basin. Fast decreases in δ^{18}Opf and IRD (and increases in δ^{13}Cpf?) in the Okhotsk Sea during climate warming appear coherent with interstadial warming in the northeastern Pacific and δ^{18}Opf reductions at Site 893A (Fig. 7). The thin-laminated sediment facies in the Santa Barbara Basin, correlated with an oxygen deficit on the bottom during interstadial events, were probably induced by weakening of sea ice formation in Okhotsk and therefore reduced NPIW ventilation in the North Pacific for warm S oscillation in the Okhotsk Sea. For the "reverse" Okhotsk Sea cycles at glacial terminations, the LDI maxima were mainly influenced by increased delivery of terrigenous matter by fluvial fluxes and than sea ice during climate warming that did not force SDW and NPIW formation. For example, the S′ 1/5 and L′ 1/5 oscillations in the Okhotsk Sea, which were significantly correlated with surface water freshening, hampered the intermediate water ventilation in the sea and N. Pacific that in turn led to bottom water stagnation and thin-laminated sedimentation in the Santa Bar-

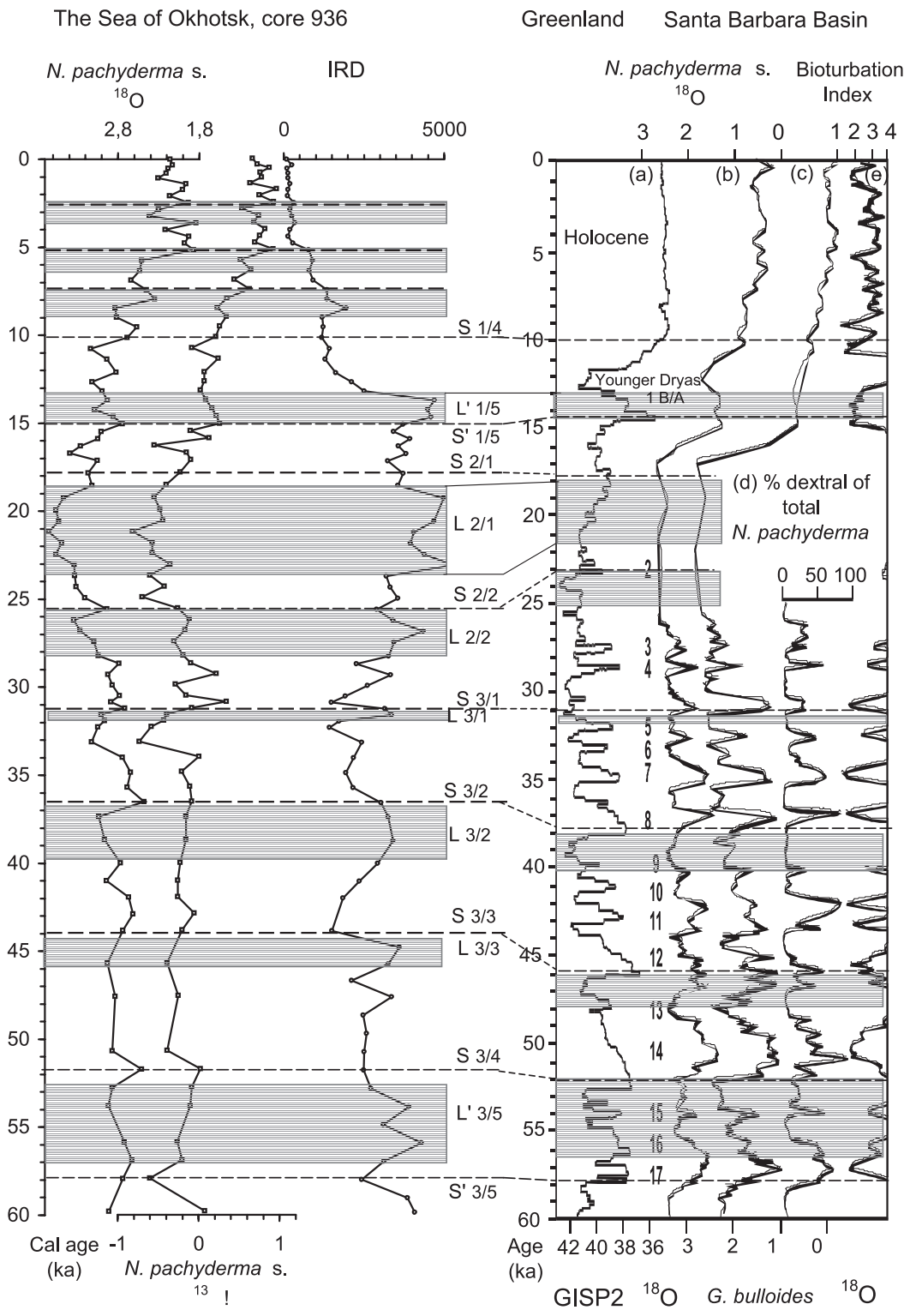
The Sea of Okhotsk, core 936
Greenland
Santa Barbara Basin
N. pachyderma s. 18O
IRD
N. pachyderma s. 18O
Bioturbation Index
2,8
1,8
0
5000
3
2
1
0
1 2 3 4
(a)
(b)
(c)
(e)
Holocene
Younger Dryas
1 B/A
S 1/4
L' 1/5
S' 1/5
S 2/1
L 2/1
S 2/2
L 2/2
S 3/1
L 3/1
S 3/2
L 3/2
S 3/3
L 3/3
S 3/4
L' 3/5
S' 3/5
(d) % dextral of total N. pachyderma
0 50 100
2
3
4
5
6
7
8
9
10
11
12
13
14
15
16
17
Cal age (ka)
-1
0
1
N. pachyderma s. 13 !
Age (ka)
42 40 38 36
3
2
1
0
GISP2 18O
G. bulloides 18O

bara Basin during the Bolling–Allerod warming (Fig. 7).

Higher resolution studies of Okhotsk Sea sediments will be required to determine the precise sequences of regional climate and sedimentation cycles, to understand in detail their nature and their correlation with changes in Greenland ice, North Atlantic, and North Pacific sediments. However, the SEI and LDI oscillations observed in core 936 have outlined the major regularities in the regional climate, Okhotsk Sea environmental and sedimentary suborbital cycles and are likely to be synchronous with Greenland D–O cycles and NE Pacific high frequency paleoceanographic changes.

3. Conclusions

The geochemical, lithological and paleontological records of core 936 from the central Okhotsk Sea display changes in hydrology, climate and sedimentation regime over the past 100 ky. Oxygen isotope stratigraphy and AMS radiocarbon data provide the basis for the core age model.

1. Large changes in grain-size, MS and sedimentation rates indicate that there were significant changes in the sedimentation regime during glacial periods. During these periods, strong increases in IRD and CF in central Okhotsk Sea sediments show an enhancement of both marine ice formation on the north shelf and of ice extent in the sea. However, the available data indicate that the main part of the sea was not covered by perennial marine ice during glaciation. Cryoaridic glacial climate conditions of the Okhotsk Sea region and increased ice formation favored a strong winter enhancement of the north shelf surface water salinity and density. These processes led to decreased water stratification and strengthened formation of SDW, SOIW, and NPIW. A strong depletion observed in the LGM δ^{13}Cpf values, of up to 1.2‰ compared with Holocene values, was probably induced by a lower productivity and reduction in air–sea CO_2 exchange during the severe LGM environment and ice cover, which resulted in a decrease in the δ^{13}C of carbon dissolved in surface water.
2. The Okhotsk records show evidence of suborbital surface hydrology, climate and sedimentology cycles. The sequence of paleoceanographic oscillations is broadly similar to those in the N. Atlantic but the hydrology and sedimentology responses to these climate changes are different. In the Okhotsk Sea, the cold stadials, indicated by diatom and pollen records, were mostly characterized by increases in IRD and CF sediment values due to a strengthening of coarse terrigenous material delivery to the basin and to increases in sea ice formation and extent. Enhanced ice formation on the north shelf, induced by climate cooling during the LDI maxima, led to an increase in shelf water density and in turn to a strengthening of SDW and SOIW formation, which is probably a driver of increased NPIW ventilation observed in the Santa Barbara Basin during cold D–O stadials. Simultaneously, the cold and dry environment and heavy ice coverage led to high δ^{18}Opf and possible low δ^{13}Cpf values in the Okhotsk Sea. Many of the terminations of these cold oscillations with high LDI values were associated with abrupt δ^{18}pf decreases, along with shifts in the diatom and pollen spectra indicating warming of the surface water and surrounding land. Reversed sequences of LDI and SEI oscillations occurred at the terminations of glacial MIS 2 and 4, when regional environmental warming and surface water freshening, associated with the negative δ^{18}Opf shift, triggered the coarse material accumulation (IRD and CF maxima). In these cases, terrigenous fluxes to the basin increased due to the climate warming and accelerated sea level rises also probably due to fluvial fluxes derived from melted mountain glaciers.

Fig. 7. Comparison of the Okhotsk Sea suborbital cycles (left side) with Greenland and Northeastern Pacific Site 893A (Santa Barbara basin) records (right side) for the last calendar 60 ky. Changes in δ^{18}O and δ^{13}C values of *N. pachyderma* s. (surface environmental indices, S oscillations) and ice rafted debris (a lithodynamic index, L oscillations) are shown for core 936 as in Fig. 2 and in Table 3. Changes in δ^{18} in Greenland ice (GISP 2), plus δ^{18}O of *N. pachyderma* s. and *G. bulloides*, % dextral of total *N. pachyderma* and bioturbation index in Site 893A (Hendy and Kennett, 2000) are on the right.

3. The SEI and LDI responses of the Okhotsk Sea to the suborbital climate changes differ from those of the N. Atlantic. During ''normal'' Okhotsk Sea cycles the increases in CF and IRD forced by climate cooling and marine ice intensification, occurred simultaneously with high δ^{18}pf. Most of the sharp δ^{18}pf decreases in the Okhotsk sediments occur at the terminations of the IRD and CF maxima, and were probably correlated with hydrologic changes related to climate warming and reductions in ice cover. We also hypothesize that an enhancement in marine ice formation and north shelf water density, induced by climate cooling during the LDI maxima, should in turn lead to strengthening of SDW, SOIW and NPIW formation.

Acknowledgements

The authors appreciate the valuable comments from three anonymous reviewers and from Dr. Keith Alverson. Thanks are due to Eben Franks for his assistance with isotope analyses and to Dr. Igor Utkin for carrying out the cluster analyses. This work was supported by NSF grant OCE93-02960, the Russian Fund for Fundamental Research 03-05-65192, Lawrence Livermore LDRD 97-ERI-009; Siberian-Far Eastern Branches of the Russian Academy of Science grant 03-2-0-00-006. AMS dating was performed in part under the auspices of the US DOE in terms of contract W-7405-Eng-48.

References

Alderman, S.E., 1996. Planktonic foraminifera in the Sea of Okhotsk: population and stable isotope analysis from sediment trap. MS thesis. Massachusetts Institute of Technology, 99.

Ananjev, G.S., Bespalyi, V.G., Glushkova, O.Yu., Ivanov, V.F., Kolpakov, V.V., Prokhorova, T.P., 1993. Stratigraphy and paleogeography of northeast Asia at Late Pleistocene. In: Velichko, A.A. (Ed.), Evolution of Landscapes and Climate of the Northern Eurasia, Late Pleistocene–Holocene Elements of Prognosis. Nauka, Moscow, pp. 59–61.

Atlas of paleoclimates and paleoenvironments of the North Hemisphere, 1992. Late Pleistocene–Holocene. In: Frenzel, B., Pecsi, M., Velichko, A.A. (Eds.), Published by Geographical Research Institute. Hungary Academy of Science, Budapest, Gustav Fischer Verlag, Stuttgard, Jena, New York, Budapest, Studgard.

Bard, E., 1998. Geochemical and geophysical implications of the radiocarbon calibration. Geochim. Cosmochim. Acta 62, 2025–2038.

Bauch, D., Carstens, J., Wefer, G., 1997. Oxygen isotope composition of living *Neogloboquadrina pachyderma* (sin) in the Arctic Ocean. Earth Planet. Sci. Lett. 146, 47–58.

Bezrukov, P.L., 1960. The bottom sediments of the Okhotsk Sea, Geological investigation in the Fareastern Seas. Tr. Inst. Okeanol. 32, 15–95 (in Russian).

Bond, G., Broecker, W., Johnsen, S., McManus, J., Labeyrie, L., Jouzel, J., Bonani, G., 1993. Correlations between climate records from North Atlantic sediments and Greenland ice. Nature 365, 143–147.

Braitseva, O.A., Melekestsev, I.V., 1974. Quaternary glaciation. In: Luchitskiy, I.B. (Ed.), Kamchatka, Kuril and Komandor Islands. Nauka, Moscow, pp. 426–438. In Russian.

Broecker, W.S., Mix, A., Andree, A., Oeschger, H., 1984. Radiocarbon measurements on coexisting benthic and planktonic foraminifera shells: potential for reconstructing ocean ventilation times over the past 20,000 years. Nucl. Instrum. Methods Phys. Res., B Beam Interact. Mater. Atoms 5, 331–339.

Broecker, W.S., Andre, M., Bonani, G., Wolfli, W., Oeschger, H., Klas, M., Mix, A., Curry, W., 1988. Preliminary estimates for radiocarbon age of deep water in glacial ocean. Paleoceanography 3, 659–669.

Charles, C.D., Fairbanks, R.G., 1992. Evidence from Southern Ocean sediments for the effect of North Atlantic deep-water flux on climate. Nature 355, 416–419.

Climate: Long-Range Investigation, Mapping and Prediction (CLIMAP), 1981. Seasonal reconstructions of the earth's surface at the Last Glacial Maximum. Map Chart Ser. Geol. Soc. Am. 36, 1–18.

COHMAP Members, 1988. Climatic changes of the last 18,000 years: observations and model simulations. Science 241, 1043–1052.

Craig, H., Gordon, I., 1965. Isotopic oceanography: deuterium and oxygen 18 variations in the ocean and marine atmosphere. Proc. Sym. Marine Lab. Occ. Publ., vol. 3. Kingston Univ. Rhode Island Press, Kingston, pp. 277–374.

Dansgaard, W., Johnson, S.J., Claussen, H.B., Dahl-Jensen, D., Gundestrup, N.S., Hammer, C.U., Hvidberg, C.S., Steffensen, D., Sveinbjornsdottir, A.E., Jouzel, J., Bond, G., 1993. Evidence of general instability of past climate from a 250 kyr ice-core record. Nature 364, 218–220.

Fairbanks, R.G., 1989. A 17,000 years glacio-eustatic sea level record: influence of glacial melting rates on the Younger Dryas event and deep-ocean circulation. Nature 342, 637–642.

Falkovski, P.G., Barber, R.T., Smetacek, V., 1998. Biogeochemical controls and feedbacks on ocean primary productivity. Science 281, 200–206.

Gladyshev, S., Martin, S., Riser, S., Figurkin, A., 2000. Dense water production on the northern Okhotsk shelves: comparison of ship-based spring–summer observations for 1996 and 1997 with satellite observations, J. Geophys. Res., 105, C11, 26,281–26,299.

Gorbarenko, S.A., 1991. Stratigraphy of the upper Quaternary sediments of the central Okhotsk Sea and its paleoceanography

using 18O and other methods. Okeanologiya 31, 1036–1042 (in Russian).

Gorbarenko, S.A., 1996. Stable isotope and lithologic evidence of late-glacial and Holocene oceanography of the Northwestern Pacific and its marginal Seas. Quat. Res. 46, 230–250.

Gorbarenko, S.A., Chekhovskaya, M.P., Southon, J.R., 1998. Detailed environmental changes of the Sea of Okhotsk Central part during the last glaciation–Holocene. Oceanology 38 (2), 277–280 (translated from Okeanologiya, 38, 2, 305–308).

Gorbarenko, S.A., Leskov, V.Yu., Tiedemann, R., Biebow, N., 2001. Climate, sea ice and productivity in the Okhotsk Sea during last 75 thousand years. Proceeding of the 16th International Symposium on the Okhotsk Sea and Sea Ice. Mombetsu, Japan, pp. 425–432.

Gorbarenko, S.A., Khusid, T.A., Basov, I.A., Oba, T., Southon, J.R., Koizumi, I., 2002a. Glacial–Holocene environment of the southeast Okhotsk Sea: evidence from geochemical and paleontological data. Palaeogeogr. Palaeoclimatol. Palaeoecol. 177/3–4, 237–263.

Gorbarenko, S.A., Nuernberg, D., Derkachev, A.N., Astakhov, A.S., Southon, J.R., Kaiser, A., 2002b. Magnetostratigraphy and tephrochronology of the upper Quaternary sediments in the Okhotsk Sea: implication of terrigenous, volcanogenic and biogenic matter supply. Mar. Geol. 183 (1–4), 107–129.

Gorbarenko, S.A., Leskov, V.Yu., Artemova, A.V., Tiedemann, R., Biebow, N., Nuernberg, D., 2003. Ice cover of the Okhotsk Sea during last glaciation and Holocene. Proc.-Russ. Acad. Sci. 388 (5), 678–682 (in Russian).

Hendy, I.L., Kennett, J.P., 2000. Dansgaard–Oeschger cycles and the California current system: planktonic foraminiferal response to rapid climate change in Santa Barbara Basin, Ocean Drilling program hole 893A. Paleoceanography 15, 30–42.

Heinrich, H., 1988. Origin and consequences of cyclic ice rafted in the Northeast Atlantic ocean during the past 130,000 years. Quat. Res. 29, 142–152.

Hofmann, M., Broecker, W.S., Lynch-Stieglitz, J., 1999. Influence of a [CO_2(aq)] dependent biological C-carbon fractionation on glacial $^{13}C/^{12}C$ ratios in the ocean. Glob. Biogeochem. Cycles 13 (4), 873–883.

Jouse, A.P., 1962. Stratigraphycal and Paleogeographycal Researches in the Northwestern Pacific. Academy of Science Press, Moscow, p. 259. In Russian.

Jouse, A.P., 1974. Diatom Flora (Fossils and Modern), vol. 1. Leningrad, Nauka, p. 404. In Russian.

Kanaya, T., Koizumi, I., 1966. Interpretation of the diatom thanatocenouses from the North Pacific applied to a study of core V 20-130. Sci. Rep. Tohoku Univ., Ser. 2 37 (2), 89–130.

Keigwin, L.D., 1998. Glacial-age hydrology of the far northwest Pacific Ocean. Paleoceanography 13, 323–339.

Keigwin, L.D., Jones, G.A., Froelich, P.N., 1992. A 15,000 year paleoenvironmental record from Meiji Seamount, far northwestern Pacific. Earth Planet. Sci. Lett. 111, 425–440.

Kimura, N., Wakatsuchi, M., 1999. Processes controlling the advance and retreat of sea ice in the Sea of Okhots. J. Geophys. Res. V. 104, CS, 11,137–11,150.

Kitani, K., 1973. An oceanographic study of the Okhotsk Sea: particularly in regard to cold waters. Bull. Far Sea Fish. Res. Lab. 9, 45–77.

Koreneva, E.V., 1957. Spore-pollen analyses of the Okhotsk Sea sediments. Proceedings-Institute of Oceanology, vol. XXII, pp. 221–251. In Russian.

Leonov, A.K., 1960. Regional Oceanography. Gidrometeoizdat, Leningrad. 766 pp. Part 1.

Lisitzin, A.P., 1994. Ice Sedimentation in world ocean. In: Bogdanov, Yu.A. (Ed.). Nauka, Moscow, p. 448. In Russian.

Lynch-Stieglitz, J., Stocker, T.F., Broecker, W.S., Fairbanks, F.G., 1995. The influence of air–sea exchange on the isotopic composition of ocean carbon: observations and modelling. Glob. Biogeochem. Cycles 9 (4), 653–665.

Martin, S., Drucker, R., Yamashita, K. 1998. The production of ice and dense shelf water in the Okhotsk Sea polynyas, Journ. Geoph. Res., 103, C12, 27,771–27,782.

Martinson, D.G., Pisias, N.G., Hays, J.D., Imbrie, J., Moore, T.C., Shackleton, N.J., 1987. Age dating and the orbital theory of the ice ages: development of a high-resolution 0 to 300,000-year chronostratigraphy. Quat. Res. 27 (1), 1–29.

Morley, J., Heusser, L.E., Shackleton, N.J., 1991. Late Pleistocene–Holocene radiolarian and pollen records from sediments in the sea of Okhotsk. Paleoceanography 6, 121–131.

Moroshkon, K.V., 1966. New scheme of the surface Okhotsk Sea currents. Oceanology 1 (4), 641–643 (in Russian).

Peng, T.-H., Broecker, W.S., 1992. Reconstruction of radiocarbon distribution in the glacial ocean. In: Taylor, R.E., Long, A., Kra, R.S. (Eds.), Radiocarbon After Four Decades, pp. 75–92.

Pokrovsky, I.M. (Ed.), 1950. Pollen Analyses. Nauka, Moscow, p. 571. In Russian.

Porter, S.C., An, Z., 1995. Correlation between climate events in the North Atlantic and China during the Last glaciation. Nature 375, 305–308.

Sancetta, C., 1981. Oceanographic and ecologic significance of diatoms in surface sediments of the Bering and Okhotsk seas. Deep-Sea Res. 28A (8), 789–817.

Sancetta, C., 1992. Primary production in the glacial North Atlantic and North Pacific. Nature 360, 249–251.

Shackleton, N.J., 1974. In: Labeyrie, J. (Ed.), Variation du Climat au Cours du Pleistocene. CNRS, Paris, pp. 9–203.

Shiga, K., Koizumi, I., 2000. Latest quaternary oceanographic changes in the Okhotsk Sea based on diatom records. Mar. Micropaleontol. 38, 91–117.

Talley, L.D., 1991. An Okhotsk sea water anomaly: implications for ventilation in the North Pacific. Deep-Sea Res., A, Oceanogr. Res. Pap. 38, S171–S190.

Talley, L.D., Nagata, Y., 1995. The Okhotsk Sea and Oyashio region, Working Group 1, North Pac. Mar. Sci. Org. (PICES), rep. 2, Sidney, B. C. 227.

Tsukada, M., 1986. Vegetation in prehistoric Japan: the last 20,000 years. In: Pearson, R.J. (Ed.), Windows on the Japanese past: Studies in Archaeology and Prehistory. Center for Japanese Studies, University of Michigan, Ann Arbor, p. 629.

Wong, C.S., Matear, R.J., Freeland, H.J., Whitney, F.A., Bychkov, A.S., 1998. WOCE Line PIW in the Sea of Okhotsk, 2, CGCs and the formation rate of intermediate water. J. Geophys. Res., 15625–15642.